

The acoustic cut-off frequency of the Sun and the solar magnetic activity cycle

A. Jiménez^{1,2}, R A García³, P L Pallé^{1,2}

ABSTRACT

The acoustic cut-off frequency—the highest frequency for acoustic solar eigenmodes—is an important parameter of the solar atmosphere as it determines the upper boundary of the p-mode resonant cavities. At frequencies beyond this value, acoustic disturbances are no longer trapped but traveling waves. Interference amongst them give rise to higher-frequency peaks—the pseudomodes—in the solar acoustic spectrum. The pseudomodes are shifted slightly in frequency with respect to p-modes making possible the use of pseudomodes to determine the acoustic cut-off frequency. Using data from GOLF and VIRGO instruments on board the SOHO spacecraft, we calculate the acoustic cut-off frequency using the coherence function between both the velocity and intensity sets of data. By using data gathered by these instruments during the entire lifetime of the mission (1996 till the present), a variation in the acoustic cut-off frequency with the solar magnetic activity cycle is found.

Subject headings: Sun: helioseismology - Sun: Oscillations

1. Introduction

Solar p-modes are essentially resonant acoustic waves that can be regarded as a superposition of outward and inwardly propagating waves that interfere constructively. At certain discrete frequencies the interference is maximally constructive yielding the eigenfrequencies of the acoustic cavity within which the p-modes propagate. The lower boundary of these resonant cavities lies at a depth inside the Sun at which the horizontal phase speed of the wave equals the local sound speed. The upper boundary of the p-mode cavities lies near the

¹Instituto de Astrofísica de Canarias, E-38205 La Laguna, Tenerife, Spain

²Departamento de Astrofísica, Universidad de La Laguna, E-38206 La Laguna, Tenerife, Spain

³Laboratoire AIM, CEA/DSM-CNRS, Université Paris 7 Diderot, IRFU/Sap, Centre de Saclay, F-91191 Gif-sur-Yvette, France

solar surface and its location depends on the frequency and wavenumber of the modes. For frequencies higher than a certain value, called the acoustic cut-off frequency (ν_{ac}), acoustic disturbances are no longer trapped and propagate as traveling waves through the chromosphere to the base of the corona. These high-frequency peaks (hereafter, pseudomodes) show a clear periodic structure beyond ν_{ac} (Jefferies et al. 1988; Libbrecht 1988; Duvall et al. 1991; García et al. 1998; Chaplin et al. 2002; Jiménez et al. 2005; Jiménez 2006). Several models have been proposed to explain the nature of the pseudomodes (Balmforth & Gough 1990; Kumar et al. 1990; Kumar 1994; Jain & Roberts 1996; García et al. 1998). Nowadays, it is generally believed that the full-disk integrated (low-degree) pseudomodes arise from geometric interference between direct waves emitted from a subphotospheric source and indirect waves produced by partial reflection on the far side of the Sun (García et al. 1998). For higher-degree modes the indirect waves are those emitted downwards toward the solar interior and refracted back to the solar surface (Kumar et al. 1990; Kumar 1994).

The acoustic cut-off frequency is given by $\nu_{ac} = c/2H_\rho \propto g/\sqrt{T_{eff}} \propto MR^{-2}T_{eff}^{-1/2}$, H_ρ being the density scale height, c the sound speed, g the gravitational field, M the mass, R the radius, and T_{eff} the temperature at the photosphere. The acoustic cut-off frequency sets the borderline between p-modes and pseudomodes and it is related with other parameters of the oscillation spectrum, for example, ν_{max} , the frequency of maximum power of the oscillations. It was conjectured by Brown et al. (1991) that the ν_{max} scales the cut-off frequency and the increasing number of observations of solar-like stars has confirmed this relation (Bedding and Kjeldsen, 2003; Stello et al. 2009). ν_{max} is associated with the coupling between turbulent convection and oscillations and results from a balance between the damping and the driving of the modes. Asteroseismic observations suggest that ν_{max} corresponds to the plateau of the damping rates (e.g., Benomar et al. 2009; Barban et al. 2009; Deheuvels et al. 2010; Ballot et al. 2011). Moreover, Belkacem et al. (2011) has addressed the question of whether the depression of the damping rates determines ν_{max} because there is a resonance between thermal time-scale in the superadiabatic region and the modal period, implying that ν_{max} does not scale only with ν_{ac} but also with the Mach number. In other stars for which stellar parameters are well known, the relation between ν_{max} and ν_{ac} could directly give the value of the Mach number in the uppermost convective layers.

The intrinsic importance of ν_{ac} increases with asteroseismology because the simple scaling relations for asteroseismic quantities have proven very useful when analyzing stellar oscillations, and these scaling relations use the Sun as a reference (Kjeldsen & Bedding 1995). For example, it is well established that to a good approximation $\Delta\nu_{n,\ell}$, the so-called large frequency separation between consecutive overtones, is proportional to the square root of the stellar density (e.g., Ulrich 1986):

$$\frac{\Delta\nu_{n,\ell}}{\Delta\nu_{n,\ell,\odot}} = \sqrt{\frac{\rho}{\rho_{\odot}}} = \frac{(M/M_{\odot})^{0.5}(T_{eff}/T_{eff,\odot})^3}{(L/L_{\odot})} \quad (1)$$

and also, following Brown et al. (1991) and Kjeldsen & Bedding (1995), we expect ν_{\max} to scale as ν_{ac} :

$$\frac{\nu_{\max}}{\nu_{\max,\odot}} = \frac{\nu_{ac}}{\nu_{ac,\odot}} = \frac{M/M_{\odot}(T_{eff}/T_{eff,\odot})^{3.5}}{L/L_{\odot}} \quad (2)$$

For the Sun $\nu_{ac,\odot} \simeq 1.7 \nu_{\max,\odot}$ (Balmforth and Gough 1990; Fossat et al. 1992). The theoretical value inferred is $\nu_{ac,\odot} \simeq 5300 \mu\text{Hz}$.

Observationally some estimates have been obtained in the past (Claverie et al. 1981; Pallé et al. 1986, 1992; Duval et al. 1991; Fossat et al. 1992) yielding different results in the range 5300–5700 μHz . Before the discovery of pseudomodes it might have been expected that a way to measure ν_{ac} would be to look for a sudden drop in the power density signal on the high-frequency side of the spectrum. All the previous observational results were obtained before the discovery of pseudomodes and probably the weak signal of the first pseudomodes were considered as p-modes. Although, in principle, the existence of pseudomodes does complicate the determination of the acoustic cut-off frequency, this in fact helps to determine it. In fact, when pseudomodes are taken into account, a lower value is obtained: $\nu_{ac} \simeq 5100 \mu\text{Hz}$ (Jiménez 2006).

The method of measuring ν_{ac} in this research is as follows. In the acoustic spectrum of the Sun, the large frequency separation between consecutive modes of the same degree $\Delta\nu_{n,\ell} = \nu_{n,\ell} - \nu_{n-1,\ell}$ is approximately equal to the inverse of the sound travel time from the upper reflection point to the lower turning point and back. This $\Delta\nu_{n,\ell}$ decreases if the lower turning point moves inward (increasing ν or decreasing ℓ), or if the outer reflection point moves outward. At a given spherical harmonic, the observed frequency spacing between peaks decreases with increasing frequency. However several authors (Kumar et al. 1994; Nigam & Kosovichev 1996) have pointed out that, between 5000 μHz and 5500 μHz , the frequency spacing increases slightly, this feature probably being associated with the acoustic cut-off frequency indicating the transition from trapped to traveling waves.

If $\Delta\nu_{n,\ell}$ increases around ν_{ac} , all the peaks with frequencies $\nu > \nu_{ac}$ will be shifted relative to the peaks with frequencies $\nu < \nu_{ac}$. Finding the frequency at which these shifts takes place would provide a good measurement of the acoustic cut-off frequency. In the present study, the coherence function between intensity and velocity signals will be used instead of the power spectra to avoid intensity contamination, as will be explained in Section 4.

The transition between p-modes and pseudomodes also could be observed in other oscillation parameters. In particular, if the phase relations (phase shifts) change for frequencies beyond ν_{ac} . These phase shifts can correspond to velocity–velocity or intensity–intensity measurements at two different spectral lines (two different formation heights), or to intensity–velocity measurements of spectral lines, narrow-band photometry, etc. For velocity–velocity (or intensity–intensity) observations, a phase difference of around 0° should be expected in the frequency range corresponding to standing (trapped) waves, i.e., the p-mode range (e.g., Fossat et al. 1992; Pallé et al. 1992; Jiménez et al. 1999). For waves with frequencies beyond ν_{ac} (the traveling wave range) a non-zero phase difference should be expected as was already measured by Staiger (1987), who found close to zero V–V phase differences between 2500 μHz and 5000 μHz , but for frequencies between 5000 μHz and 7000 μHz he also found that the phase difference changes almost linearly, and that these values were in good agreement with theoretical values calculated by Schmieder (1977, 1978) under the assumption that vertically traveling waves exist beyond the acoustic cut-off frequency.

For intensity–velocity observations the phase differences give information about the adiabatic or non-adiabatic behavior of the solar atmosphere. In the adiabatic case a value of -90° or $+90^\circ$ (depending on the sign convention for upward/downward positive velocity) is expected for the p-mode range and a value of 0° for a model close to isothermal (Marmolino & Severino 1991). For non-adiabatic conditions the phase differences change with frequency depending on the model used (Gough 1985; Houdek et al. 1995). The results of Jiménez (2002) show that in the p-mode range the I–V phase differences do not show an exactly adiabatic behavior but one that is close to it. Our concern in the present investigation is that these I–V phase differences in the p-mode range are found to be close to -90° , are roughly constant with frequency, and have no dependence on solar activity (Jiménez et al. 2002).

The theoretical results of Schmieder (1978) show that the I–V phase differences for frequencies beyond ν_{ac} also change almost linearly in the frequency range between 5000 μHz and 6500 μHz because of the traveling nature of the waves. Taking into account the different I–V phase relationships between p-modes and pseudomodes it would be interesting to know how I–V phase differences are affected by the transition between standing and traveling waves and determine whether this effect corresponds to ν_{ac} .

2. Instrumentation

2.1. VIRGO/SPM (Intensities)

The Solar Photometers (SPM) of the Variability of solar IRradiance and Gravity Oscillations (VIRGO) package (Fröhlich et al. 1995, 1997) aboard the Solar and Heliospheric Observatory (SOHO) mission, consists of three independent photometers, centered around 402, 500 and 862 nm (the blue, green, and red channel respectively). They measure the spatially integrated solar intensity over a 5 nm bandpass at a one minute cadence. The data obtained by the VIRGO/SPM instrument over the mission have been of uniformly high quality, whether before or after the loss of contact with the spacecraft for several months in 1998.

2.2. GOLF (Velocity)

The Global Oscillations at Low Frequency (GOLF) instrument on board SOHO (Gabriel et al. 1995, 1997) is a resonant scattering spectrophotometer that measures the line-of-sight velocity between the Sun and the spacecraft using the sodium doublet. It uses the same technique as other ground-based helioseismic networks such as the International Research on the Interior of the Sun (IRIS, Fossat 1990) and the Birmingham Solar Oscillations Network (BiSON, Broomhall et al. 2009). The GOLF window was opened in 1996 January and became fully operational by the end of that month. Over the following months, occasional malfunctions in its rotating polarizing elements were noticed that led to the decision to stop them in a predetermined position; truly non-stop observations began by 1996 mid-April (García et al. 2005). Since then, GOLF has been continuously and satisfactorily operating in a mode unforeseen before launch, showing fewer limitations than anticipated. The signal, then, consists of two close monochromatic photometric measurements in a very narrow band (25 mÅ) on a single wing of the sodium doublet (García et al. 2005). This signal has been calibrated as velocity and is indeed similar in nature to other known velocity measurements, such as those of IRIS and BiSON (Pallé et al. 1999). The sampling of the GOLF data used in this paper is 60 s. Before the 1998 loss of contact with the SOHO spacecraft (June 1998), the GOLF instrument was operated using the blue wing of the sodium line. When thereafter contact with the spacecraft was reestablished (October 1998) the instrument operating mode was switched to the red wing of the line until November 2002. Since then, it was switched back to the blue wing. In Table 1 we summarize the GOLF working configurations as well as the associated duty cycle of each series.

Table 1: Time series number, dates, and sodium wing observed by GOLF in each period and mean duty cycle (DC) of the time series used.

| Time series | Dates Interval | Na wing | DC |
|-------------|---------------------------|---------|-------|
| 0-19 | April 96 to June 98 | blue | 91.7% |
| 20-33 | June 98 to November 2002 | red | 99.4% |
| 34-85 | November 2002 to May 2010 | blue | 97.6% |

3. Data sets

In this study we use VIRGO/SPM (three color) intensity and GOLF velocity time series recorded for the last ~ 15 years. A total of 85 time series of 800 consecutive days –covering the period April 1996 till May 2010– have been analyzed. Each one is shifted 50 days with respect to the previous one. Each 800-day time series is later sub-divided into 4-day time series (5760 one-minute sampled points, with a frequency resolution of $2.89 \mu\text{Hz}$). Their corresponding power spectra and the bivariate parameters (coherence and phase differences) are computed and the results averaged (time series with more than 500 missing points are excluded). Figure 1 shows a sample of the power spectra of the three channels of VIRGO/SPM (red, green, and blue), and the GOLF spectrum from $3000 \mu\text{Hz}$ (including the high frequency part of the 5-minute oscillations band) to the Nyquist frequency. The periodic structure of the pseudomodes is clearly seen in all the signals.

To study the transition frequency range between p-modes and pseudomodes where ν_{ac} should be located, the coherence and phase shift between the intensity and velocity signals will be used. In phase analyses the correct timing of the temporal series is a critical issue that should be carefully addressed. In the present case, VIRGO data timing is very well determined and remained stable throughout the mission. In contrast, GOLF timings presented some shifts during the mission and required proper correction. The corrections introduced were satisfactory (see García et al. 2005 for more details) and time series ready to be used in the combined VIRGO/GOLF analysis were then produced (Jiménez et al. 1999; Jiménez 2002). In fact, additional tests have been performed in the present study and the resulting maximum errors in the computed I-V phase difference GOLF/VIRGO for the largest possible timing error ($+3.3144$ s) turns out to be smaller than 8° in the frequency band of interest (3.5 to 7 mHz).

4. Data analysis

The method we used to compute the coherence, and the phase differences is described in Koopmans (1974). Briefly, let A and B be two time series of length T and $\sin A$, $\cos A$, $\sin B$, and $\cos B$ be the sine and cosine amplitudes of the spectra for series A and B . The power spectral densities, $P_A(\nu)$ and $P_B(\nu)$, the co-spectral density, $C_{AB}(\nu)$, the quadrature spectral density, $q_{AB}(\nu)$, and the complex cross-spectral density $P_{AB}(\nu)$ are defined as:

$$P_A(\nu) = \frac{T}{2}[\sin^2 A(\nu) + \cos^2 A(\nu)] \quad (3)$$

$$P_B(\nu) = \frac{T}{2}[\sin^2 B(\nu) + \cos^2 B(\nu)] \quad (4)$$

$$C_{AB}(\nu) = \frac{T}{2}[\sin A(\nu) \sin B(\nu) + \cos A(\nu) \cos B(\nu)] \quad (5)$$

$$q_{AB}(\nu) = \frac{T}{2}[\sin A(\nu) \cos B(\nu) - \sin B(\nu) \cos A(\nu)] \quad (6)$$

$$P_{AB}(\nu) = C_{AB}(\nu) - iq_{AB}(\nu) \quad (7)$$

The coherence (the analogue of the linear correlation coefficient between the two time series A and B in linear regression analysis) and the phase difference, $\Delta\phi_{AB}(\nu)$ between series A and B are given by:

$$Coh_{AB}^2(\nu) = \frac{\langle C_{AB}(\nu) \rangle^2 + \langle q_{AB}(\nu) \rangle^2}{\langle P_A(\nu) \rangle \langle P_B(\nu) \rangle} = \frac{|\langle P_{AB}(\nu) \rangle|^2}{\langle P_A(\nu) \rangle \langle P_B(\nu) \rangle} \quad (8)$$

$$\Delta\phi_{AB}(\nu) = \tan^{-1}\left(\frac{\langle q_{AB}(\nu) \rangle}{\langle C_{AB}(\nu) \rangle}\right) \quad (9)$$

where $\langle .. \rangle$ stands for a 5-bin smoothing of the respective functions. The length of the smoothing is not too critical, but needs to be chosen adequately. If it is too short, the parameters are noisy from bin to bin, and if it is too large the frequency resolution is lost. After several tests varying the length of the smoothing we concluded that 5 bins is the best trade-off for this frequency range.

The errors for the phase difference are given by:

$$\epsilon_{\Delta\phi_{AB}}(\nu) = \sin^{-1}\left(\sqrt{\frac{1 - Coh_{AB}^2(\nu)}{(2n - 2)Coh_{AB}^2(\nu)}} t_{2n-2}\left(\frac{\alpha}{2}\right)\right), \quad (10)$$

where n represents the equivalent degrees of freedom (EDF), $t_{2n-2}(\alpha/2)$ the Student t -distribution, and α the confidence level at which the errors are computed ($\alpha=0.8$ for phase differences).

After computation of the power spectra and bivariate parameters for each pair of 4-day time series, these are averaged to obtain four final power spectra (one for each of the three VIRGO/SPM channels and one for GOLF) and three sets of bivariate parameters (coherence and phase shift) between each of the VIRGO/SPM channels with GOLF. The power spectra and bivariate parameters of 200 consecutive 4-day time series are thus averaged obtaining the results for the first 800-day time series and this is repeated for the 85 subseries of 800 days.

The VIRGO signals show a peak (highest in the green channel) at just 5555 μHz (see Figure 1) corresponding to 3 minutes. This is precisely the period of the calibration reference used by the Data Acquisition System (DAS) of VIRGO. This is an electronic artifact that in principle could contaminate the determination of the acoustic cut-off frequency but, as will be seen in the following sections, it is not a problem because the coherence and phase-shift are not affected by this artifact. Indeed, this signal is not present in the GOLF data, therefore it yields a low value of the coherence at this frequency. The use of power spectra to determine the acoustic cut-off frequency requires special care in the treatment of this instrumental signal, but does not affect the coherence and phase-shift on which this work is based.

Figure 2 shows two power spectrum densities (PSD), in the range 3000 to 7000 μHz , computed from an example of two 800-day subseries (one in intensity and one in velocity). We also show the resultant bivariate parameters. The coherence function has its maxima just where the p-mode maxima lie. This means that the coherence has the relative maxima at the frequencies in which both the intensity and velocity signals are coherent. In the pseudomode range $\nu > 5000$ μHz the coherence function also shows some maxima because of the presence of pseudomodes in both signals. The visibility of the peaks in the coherence function is much higher than in the power spectra.

The bottom plot of Figure 2 shows the phase difference between the intensity and the velocity signals. The exact value of the phase difference is at the frequencies where the coherence function has its maxima, usually close to the maxima of the phase difference function. The phase differences between I-V p-modes are close to the adiabatic value of

–90 degrees (see Jiménez 2002) but beyond the acoustic cut-off frequency $\sim 5000 \mu\text{Hz}$ a change takes place: the phase differences decrease approximately linearly in this region. The frequency at which this different behavior of the phase difference takes place will be studied in Section 6.

5. Determination of the acoustic cut-off frequency

As explained in the introduction, a change in the value of the frequency spacing between p-modes and pseudomodes is expected because of the increase in the large frequency separation around the acoustic cut-off frequency. To find where this frequency spacing change starts to take place, a convenient definition of the acoustic cut-off frequency is derived and adopted in this section.

An exponentially modulated sine wave is fitted to the coherence function between 3500 and 5500 μHz to take into account the decreasing amplitude of p-modes in this frequency range. In Figure 3a the coherence function (black line) is plotted between 3500 and 6500 μHz , together with the modulated sine wave (blue line) but extended to 6500 μHz .

The shape of the solar signal in the pseudomode region (between 5000 μHz and 6500 μHz) is like a sine wave. Thus a single sine wave is fitted to the coherence function between 5000 and 6500 μHz . This second fit is also plotted in Figure 3a (red line) and extended to lower frequencies, down to 3500 μHz . The interval from 5000 μHz to 5500 μHz is used in both fits because it is the interval where the acoustic cut-off frequency is expected to be found and also because, obviously, it is not possible to separate p-modes from pseudomodes before finding the acoustic cut-off frequency (in several tests this interval has been slightly changed and the same results were obtained).

The maxima of the three curves—coherence, modulated sine wave, and single sine wave—have been computed and plotted in Figure 3a, where black, blue, and red circles correspond to the frequencies of the respective maxima of these variables. Up to 5000 μHz the coherence function and the fitted modulated sine wave are in phase and their maxima have the same frequencies. No blue circles are visible below 5000 μHz because they are over-plotted by the black ones. Around 5000 μHz the coherence function starts to shift to higher frequencies and the maxima of the fitted modulated sine wave are delayed with respect to those of the coherence function. Blue circles then become visible and the coherence shift increases with frequency, being out of phase (maxima of the coherence coincides with minima of the fitted modulated sine wave) between 6000 and 6500 μHz .

In the pseudomode region, just the opposite effect takes place. The coherence function

and the fitted single sine wave go out of phase from higher to lower frequencies. From 6500 to around 5000 μHz the coherence and the fitted single sine wave are in phase and their maxima have the same frequencies. From around 5000 μHz to lower frequencies the coherence function begins to delay with respect to the fitted single sine wave, and in fact they are out of phase (the maxima of the coherence coincides with the minima of the fitted function) between 4000 and 3500 μHz (red circles are well visible).

To look in detail at these two opposing effects, the frequency differences between the maxima of Figure 3a are computed; that is, the frequency differences between the maxima of the coherence function and the maxima of the fitted modulated sine wave and between the maxima of the coherence function and the maxima of the single sine wave. In Figure 3b blue circles correspond to the former (p-modes) and red squares to the pseudomodes.

Blue circles have an approximately constant value close to zero in the frequency range where the p-mode coherence signal is in phase with the fitted function; that is, from 3500 up to ~ 5000 μHz . At this frequency the coherence shifts to higher frequencies and the values of the maxima differences increase up to 38 μHz at the frequencies where coherence and fitted function are out of phase.

The frequency differences between the maxima of the coherence and the maxima of the single sine wave fitted to the pseudomode range (red squares) are out of phase in the p-mode frequency range. From a value of around 40 μHz at 3500 μHz , these differences decrease with frequency up to, again, around 5000 μHz . From this frequency the differences have an approximately constant value in the frequency range where the coherence and the fitted function are in phase. This constant value is close to zero but with some dispersion, probably because of the irregular shape of the pseudomodes.

At this point, we define the acoustic cut-off frequency value as the crossing point of both frequency differences shown in Figure 3b. This crossing point is the frequency at which, hypothetically, the maxima of both fitted functions and the maxima of the coherence coincide.

Looking around 5000 μHz in Figure 3b, the blue points are always below the red ones for lower frequencies and always above for higher frequencies. The frequency interval between the transition of blue points from below to above the red points (indicated by a hexagon) is the frequency interval of the acoustic cut-off value. These two limits are the lower and upper limits of ν_{ac} . A more accurate determination of ν_{ac} is performed by fitting two parabolas (one for the red points and one for the blue points) in the interval from 4500 to 5500 μHz and computing the their crossing frequency point. This is considered as the best feasible determination of ν_{ac} .

The acoustic cut-off frequency for low-degree modes found with this method is lower than indicated in previous observations in which a wide range of values were found between 5300 and 5700 μHz . All these previous determinations (Claverie, et al. 1981; Pallé et al. 1986, 1992; Duval et al. 1991; Fossat et al. 1992) were performed using ground-based observations, with different techniques, and with a poor visibility of the pseudomodes. A suggested explanation for these discrepancies could be the higher quality of the SOHO space-based data and the possibility that a lack of good visibility of the pseudomodes might require different techniques to consider the trace of the first pseudomodes as a p-mode signal.

From the analysis of this section we can compute the evolution with time of the mean large frequency separation for p-modes and pseudomodes. From the exponentially modulated sine wave fitted to the coherence function (p-mode range), we can extract the separation for p-modes and from the sine wave fitted to the coherence function (the pseudomode range) we can extract the separation for pseudomodes. In Figure 4, we plot these differences (filled circles for p-modes and open squares for pseudomodes). An almost constant difference in the mean $\Delta\nu_{n,\ell}$ is observed for p-modes and pseudomodes, with a difference around 2 μHz . The higher dispersion of $\Delta\nu_{n,\ell}$ for pseudomodes before 2002–2003 is probably the influence of the rising part of the solar activity cycle which makes the pseudomode range noisier where the S/N ratio is much lower than that for the p-modes.

6. The acoustic cut-off frequency and the solar activity cycle

The final values of the acoustic cut-off frequency, computed from the 800-day time series described in Section 3, are shown in Figure 5 for the three VIRGO/SPM photometers and for GOLF. The values of the acoustic cut-off obtained as the crossing point of the two parabolic segments (Figure 3b) are represented by black dots whereas the two limits (the frequency interval between the transition of blue points from below to above the red points in Figure 3b) are shaded in gray.

The acoustic cut-off for the three channels of VIRGO/SPM (red, green, and blue), together with the solar radio flux integrated as the time series used for the ν_{ac} computations, are plotted in Figure 6, where a clear correlation between ν_{ac} and the solar activity cycle can be seen. We computed different correlation indices between the acoustic cut-off frequency of the red, green, and blue VIRGO/SPM channels, and the solar radio flux: the Pearson coefficient correlation (P), the Spearman rank correlation (S) and its two-sided significance P_s (probability of having a null correlation). These correlations are shown in Table 2, from which we may conclude that there is a high positive correlation between the ν_{ac} and the magnetic activity.

The p-mode frequency shift produced by magnetic activity cannot explain the variation observed in ν_{ac} , as the amount of this shift is of the order of $0.4 \mu\text{Hz}$ (Broomhall et al. 2009; Salabert et al. 2011), much smaller than our present bin width ($2.89 \mu\text{Hz}$), and the obtained amplitude of the ν_{ac} variation is around $100 \mu\text{Hz}$.

As mentioned in the introduction we also investigate how the I-V phase differences could be affected by the transition between p-modes and pseudomodes. Figure 7 shows the phase differences between $4000 \mu\text{Hz}$ and $6000 \mu\text{Hz}$ for three different time series. As explained in Section 4, the I-V phase differences between p-modes does not correspond to the adiabatic value (-90 degrees) but is close to it, reaching the higher values close to the acoustic cut-off frequency. In the pseudomode regions the phase differences decrease almost linearly, giving a parabolic shape to the I-V phase differences in this frequency interval ($4000 \mu\text{Hz}$ to $6000 \mu\text{Hz}$). The black points in each of the three plots of Figure 7 are the values of the phase difference function at the frequencies where the coherence function has its maxima; i.e., the phase differences between p-modes and between pseudomodes. The two parabolic lines in each plot are two fitted parabolas, one using the phase difference values (black dots) and the other using the whole phase difference function. The purpose of these fits is to know the position of the maxima of these two parabolas. From a first inspection, it is clear that the maxima of the first plot (a) and third plot (c) are similar, whereas the maxima of the middle plot (b) seem to be at higher frequencies. The first and third plots correspond to time series close to the minimum of solar activity, a) in 1996 and b) in 2009 and the middle plot correspond to a time serie close to the maximum of solar activity (2001). This analysis have been done for the 85 time series and the maxima of the two parabolas computed is plotted in Figure 8. The different colors correspond to the red, green, and blue channels of VIRGO/SPM and the black line is the solar radio flux integrated in the same subseries. Although the values plotted in Figure 8 cannot be considered as a direct measurement of the acoustic cut-off frequency, the phase difference function at these frequencies is related to

Table 2: Results from the correlations between the acoustic cut-off frequency and the solar radio flux, The Pearson coefficient correlation (P), the Spearman rank correlation (S) and its two-sided significance P_s (probability of having a null correlation) for the red, green, and blue VIRGO/SPM channels.

| Channel | P | S | P_s |
|---------|------|------|------------------------|
| Red | 0.86 | 0.84 | 1.67 E^{-23} |
| Green | 0.85 | 0.88 | 1.15 E^{-28} |
| Blue | 0.77 | 0.75 | 1.79 E^{-16} |

the presence of pseudomodes, and therefore with ν_{ac} ; hence, it follows the same correlation with the solar activity cycle as the values of ν_{ac} computed previously (Figure 6).

A detailed analysis of Figure 8 suggests a delay between the solar cycle and the position of the maxima of the parabolic fits to the phase difference functions. By plotting these values as a function of the solar radio flux we obtain the results shown in Figure 9 (for the green channel). Black symbols correspond to the maxima of Figure 8 for the fit to the whole phase difference function. The filled circles correspond to the ascending part of the cycle, and the open squares to the descending one. The maxima of the phase difference do not have a linear dependence on the solar cycle and the path in the ascending and descending part of the cycle are different. This is a “hysteresis” cycle which was already found in other p-mode parameters as the frequency shifts (e.g., Jimenez-Reyes et al. 1998). On the other hand, we also plot the acoustic cut-off as a function of the solar radio flux (in red), which follows a linear relation with the solar cycle (the straight red line is the resultant fit). In Table 3 we show the slope of the straight lines for the three channels of VIRGO/SPM.

7. Conclusions

In this work we have determined the acoustic cut-off frequency of the Sun, ν_{ac} , using pseudomode properties, in particular, the increase in the large separation around ν_{ac} that set the limit between p-modes and pseudomodes. Instead of power spectra we used the coherence function obtained with bivariate analysis between simultaneous intensity and velocity time series. Our results show that the value of ν_{ac} is lower than the theoretical value and also lower than previous determinations in which power spectra were used without taking into account the influence of the pseudomodes. The acoustic cut-off frequency has been determined along the solar activity cycle during the 15 years of SOHO measurements. The results show a clear correlation of ν_{ac} with magnetic activity, the mean value being around 5000 μHz . The variation between maximum and minimum is around 100–150 μHz . This relation between ν_{ac} and magnetic activity is linear.

Table 3: Slope of the linear fits to ν_{ac} as function of solar radio flux.

| Channel | Slope ($\text{W}/\text{m}^2/\text{Hz}/\mu\text{Hz}$) |
|---------|--|
| Red | 0.759 |
| Green | 0.680 |
| Blue | 0.654 |

The exact determination of the solar ν_{ac} and its variation during the solar cycle is important not only intrinsically, but also for its asteroseismic implications. On the one hand, scaling relations from solar values are widely generalized in asteroseismology and these relations use the maximum of the p-mode hump, which is related with ν_{ac} . On the other hand, magnetic activity cycles have begun to be detected in other stars by means of asteroseismology (García et al. 2010). Thus, a better knowledge of the behavior of the cut-off frequency would improve our understanding of other stars.

To apply the method used in this research to other stars, simultaneous intensity and velocity observations are required. The KEPLER satellite provides photometric measurements of thousands of solar-like stars, but from different ground-based campaigns such as the forthcoming SONG (Stellar Observations Network Group), simultaneous velocity data could be obtained at least for a couple of bright stars observed by KEPLER to try to determine the probable existence of pseudomodes and find the acoustic cut-off frequency in solar-like stars.

The dependence of ν_{ac} with magnetic activity is also verified by the position of I-V phase difference maxima in the interval from 4000 μHz to 6000 μHz , indicating a transition from p-modes to pseudomodes. This transition is also correlated with the solar activity cycle in the same sense but with a hysteresis cycle pattern that could be a manifestation of surface effects or due to time-delayed responses to a single phenomenon located deeper in the Sun.

This work was funded by the Spanish grant AYA2004-04462 and AYA2010-17803 of the Ministry of Science. RAG acknowledges the support of the CNES grant at the SAP CEA/Saclay. The GOLF and VIRGO instruments benefit from the quiet and well run SOHO platform built by Matra–Marconi Space. SOHO is an international collaboration program of the European Space Agency (ESA) and the National Aeronautics Space Administration (NASA). VIRGO and GOLF represent the cooperative efforts of many individual scientists and engineers at several institutes in Europe and the USA to whom we are deeply indebted.

REFERENCES

- Ballot, J., Gizon, L., Samadi, R., et al. 2011, *A&A*, 530, A97
- Balmforth, N. J., & Gough, D. O. 1990, *ApJ*, 362, 256
- Barban, C., Deheuvels, S., Baudin, F., et al. 2009, *A&A*, 506, 51
- Bedding, T. R. and Kjeldsen, H. 2003, *PASA*, 20, 203

- Belkazen, K., Goupil, M.J., Dupret, M.A., Samadi, R., Baudin, F., Noels, A. and Mosser, B. 2011 A&A, 530, A142
- Benomar, O., Baudin, F., Campante, T. L., et al. 2009, A&A, 507, L13
- Broomhall, A.M., Chaplin, W. J., Davies, G. R., Elsworth, Y., Fletcher, S. T., Hale, S. J., Miller, B., New, R. 2009, MNRAS, 396, L100
- Brown, T. M., Gilliland, R. L., Noyes, R. W., Ramsey, L. W., 1991, ApJ, 368, 599
- Chaplin, W. J., Elsworth, Y., Isaak, G. R., Miller, B. A., & New, R. 2000, MNRAS, 313, 32
- Chaplin, W. J., et al. 2002, in Local and Global Helioseismology: The Present and Future, ed. H. Sawaya-Lacoste (Noordwijk: ESA SP- 517), 247
- Claverie, A., Isaak, G.R., McLeod, C.P., van der Raay, H.B. & Roca Cortés, T. 1981, Sol. Phys., 74, 51
- Deheuvels, S., Bruntt, H., Michel, E., et al. 2010, A&A, 515, A87
- Duvall, T. L., Harvey, J. W., Jefferies, S., M., & Pomerantz, M., A. 1991, ApJ, 373, 308
- Fossat, E. 1990, Sol. Phys., 133, 1
- Fossat, E. et al. 1992, A&A, 266, 532
- Fröhlich, C., et al. 1995, Sol. Phys., 162, 101
- Fröhlich, C., et al. 1997, Sol. Phys., 170, 1
- Gabriel, A. H., et al. 1995, Sol. Phys., 162, 61
- Gabriel, A. H., et al. 1997, Sol. Phys., 175, 207
- García, R. A., Pallé, P. L., Turck-Chièze, S. et al. 1998, ApJ, 504, L51
- García, R. A., et al. 2004, in Helio- and Asteroseismology: Towards a Golden Future, ed. D. Danesy (Noordwijk), ESA SP-559, 432
- García, R. A., Turck-Chièze, S., Boumier, P., et al. 2005, A&A, 442, 385
- García, R.A., Mathur, S., Salabert, D., et al. 2010, Science, 329, 1032
- Gough, D. 1985, Proc. ESA Workshop on Future Missions in Solar, Heliospheric and Space Plasma Physics, Noordwijk, The Netherlands, ed. E.Rolfe & B.Battrick, ESA SP 235, 183

- Houdek, G., Balmforth, N. J., & Christensen-Dalsgaard, J. 1995, Proc. Fourth SOHO Workshop: Helioseismology, Pacific Grove, California, ed. J.T. Hoeksema, V. Domingo, B. Fleck & B.Batrick, ESA SP-376, 447
- Jain, R., & Roberts, B. 1996, ApJ, 456, 399
- Jefferies, S. M., et al. 1988, in Seismology of the Sun and Sun-like Stars, ed. E. Rolfe (Noordwijk: ESA SP-286), 279
- Jiménez, A., Roca Cortés, T., Severino, G., & Marmolino, C. 1999, ApJ, 525, 1042
- Jiménez, A. 2002 ApJ, 581, 736
- Jiménez, A., Jiménez-Reyes, S.J., & García, R.A., 2005, ApJ, 623,1215.
- Jiménez, A. 2006, ApJ, 646, 1398
- Jiménez-Reyes, S.J., Régulo C., Pallé P.L. & Roca Cortés T., 1998 A&A, 329, 1119
- Kjeldsen, H. and Bedding, T. R. 1995, A&A, 293, 87
- Koopmans, L., H. 1974, The Spectral Analysis of Time Series (New York: Academic)
- Kumar, P., et al. 1990, in Lecture Notes in Physics, 367, Progress of Seismology of the Sun and Stars, ed. Y. Osaki and H. Shibahashi (Heidelberg: Springer), 87
- Kumar, P. 1994, ApJ, 428, 827
- Kumar, P., Fardal, M.A., Jefferies, S.M., Duvall, Jr., Harvey, J.W.& Pomerantz,M.A. 1994, ApJ, 422, L29
- Libbrecht, K. G. 1988, ApJ, 334, 510
- Marmolino, C., & Severino, G. 1991, A&A, 242, 271
- Nigam, R. & Kosovichev, A.G. 1996, Bull. Astr. Soc. India, 24, 195
- Pallé, P. L. et al. 1986, A&A, 169, 313
- Pallé, P. L., Régulo, C., Roca Cortés, T., Sanchez Duarte, L. & Schmider, F.X. 1992, A&A, 254, 348
- Pallé, P. L., et al. 1999, A&A, 341, 617
- Salabert, D., García, R. A., Pallé, P. L., Jiménez, A. 2011, JPhCS, 271, 012030

Schmieder, B. 1977, Sol. Phys., 54, 269

Schmieder, B. 1978, Sol. Phys. 57, 245

Staiger, J. 1987, A&A, 175, 263

Stello, D., Chaplin, W. J., Basu, S., Elsworth, Y. and Bedding, T. R. 2009, MNRAS, 400, L80

Ulrich, R.K., 1986, ApJ, L37-L40

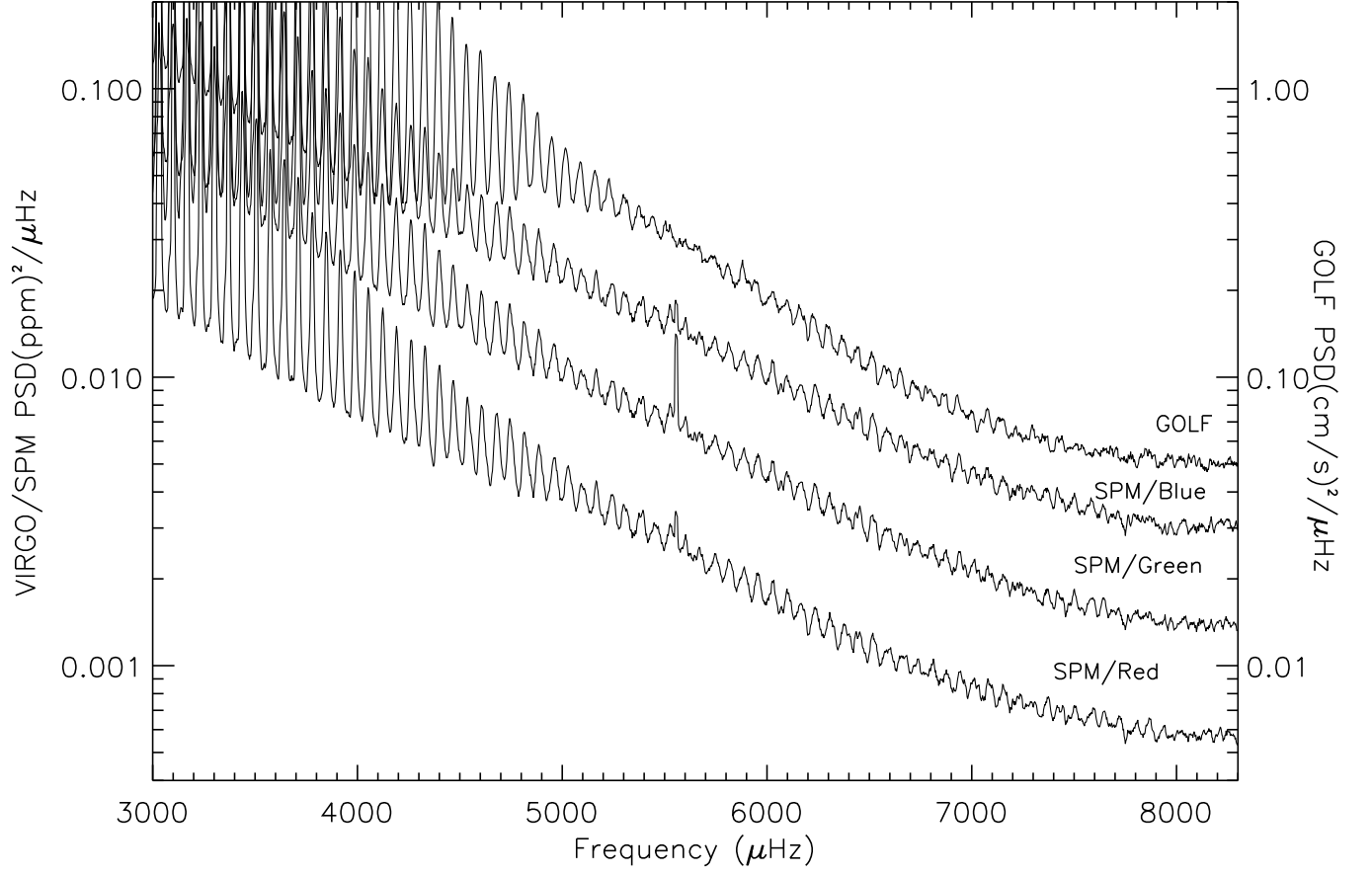


Fig. 1.— Smoothed power spectra showing the clear periodic structure of pseudomodes for the signals used in this work. Bottom to top: The red, green, and blue channels of VIRGO/SPM, and the GOLF spectra.

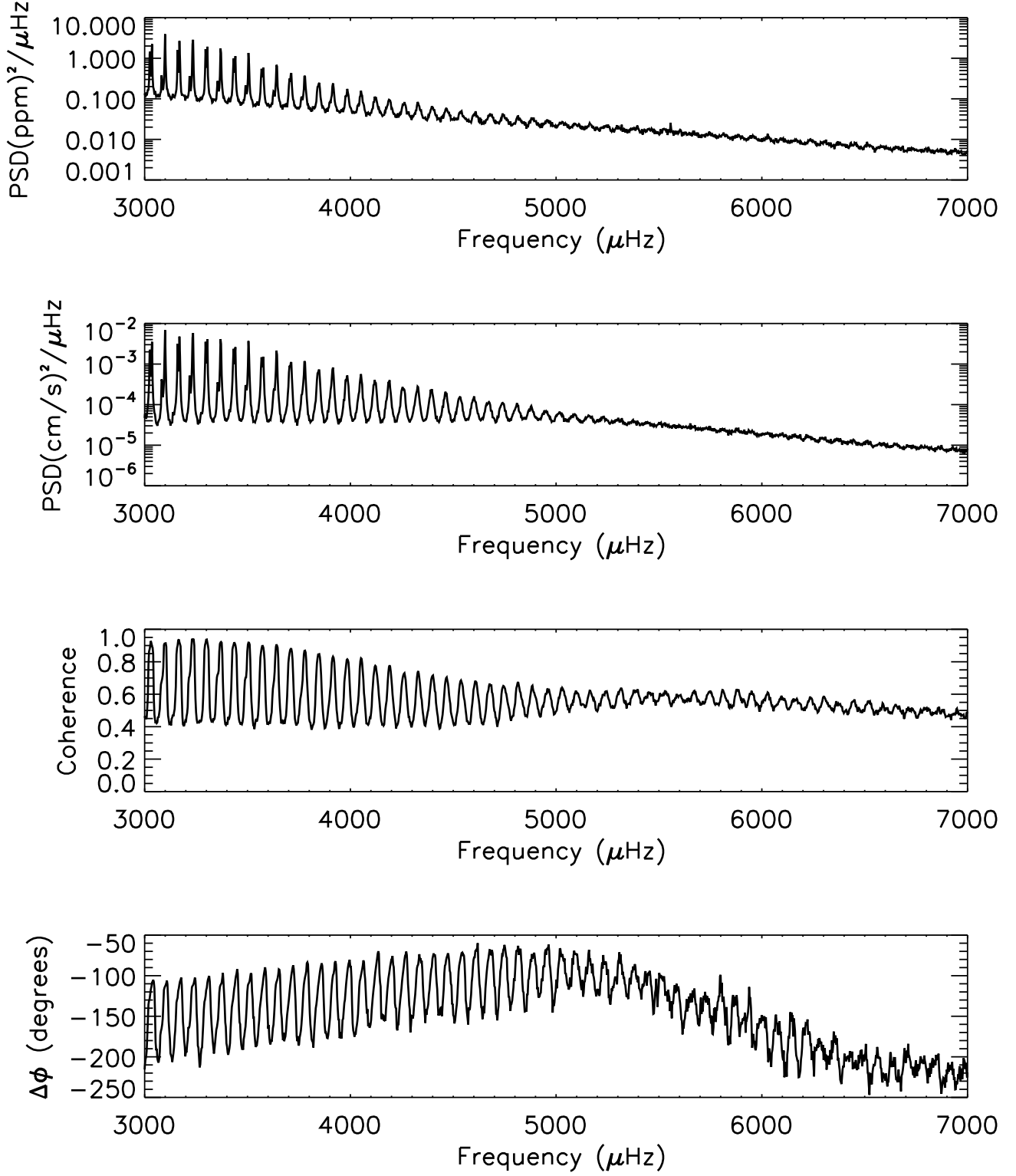


Fig. 2.— Intensity and velocity power spectra of one of the time series used and the corresponding bivariate parameters between both time series, coherence and phase difference.

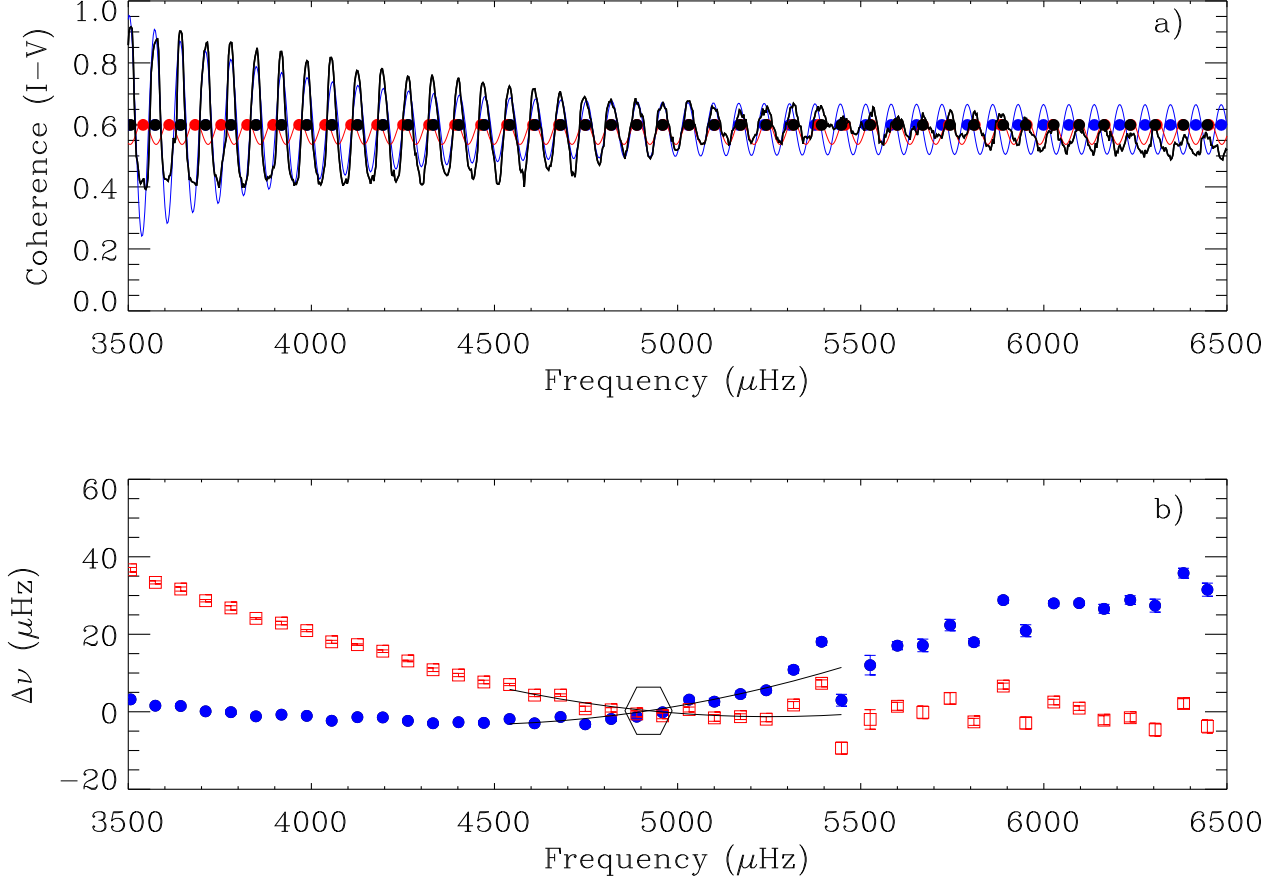


Fig. 3.— a) Black line: coherence function. Blue line: Exponentially decaying sine wave fitted to the coherence function between 3500 μHz and 5500 μHz (end of the p-mode range) and extended to 6500 μHz . Blue and black filled circles are the maxima of the fitted sine wave and coherence function respectively. Note how the coherence shifts to higher frequencies from ~ 5000 μHz onwards. Red line: Single sine fitted to the frequency range between 5000 μHz and 6500 μHz (pseudomode range) and plotted extended to 3500 μHz . Red and black filled circles are the maxima of the fitted sine and the coherence function. b) Blue circles: frequency differences between the maxima of the coherence function and the fitted (3500–5500 μHz) exponentially modulated sine wave. Red squares: frequency differences between the maxima of the coherence function and the fitted sine (5000–6500 μHz). Two parabola segments are fitted to the central part to get an estimation of ν_{ac}

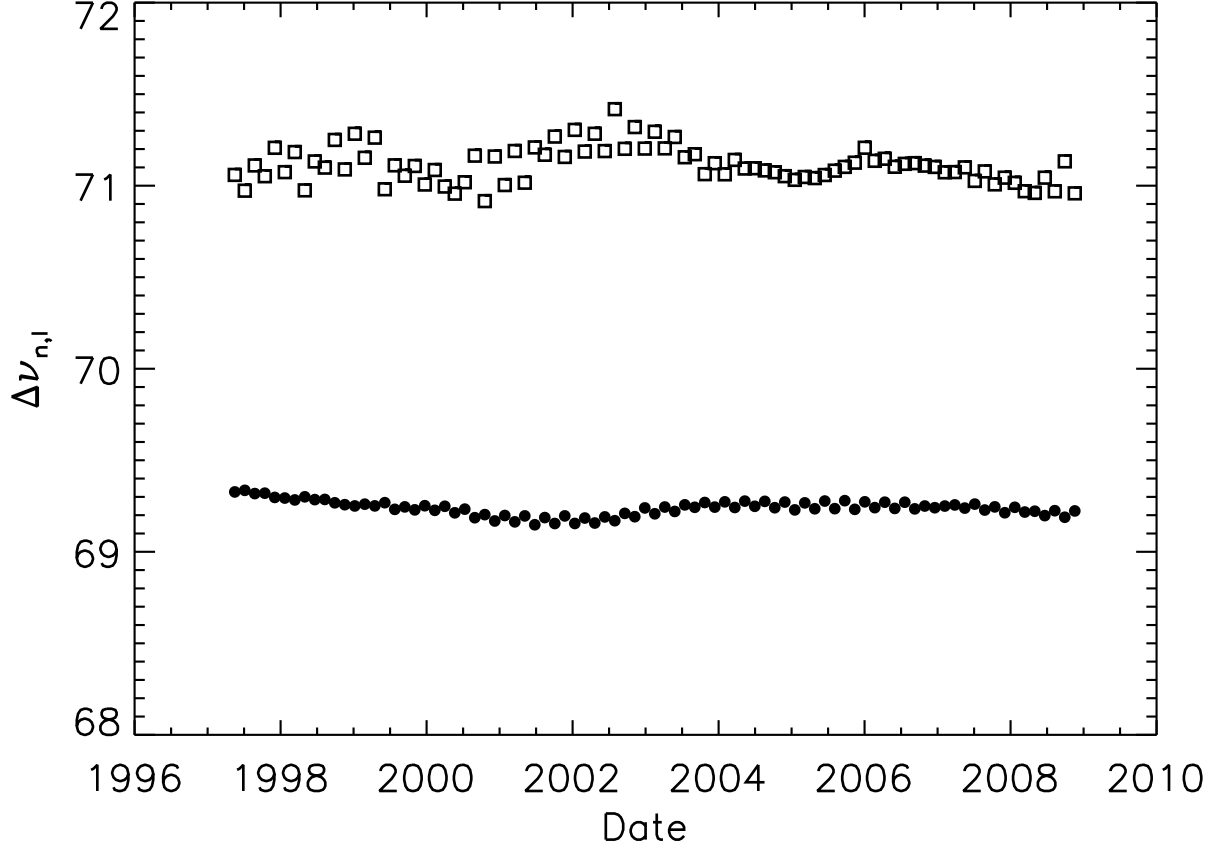


Fig. 4.— Time variation in the mean frequency separation $\Delta\nu_{n,\ell}=\nu_{n,\ell}-\nu_{n-1,\ell}$ for p-modes (filled circles) and for pseudomodes (open squares) obtained from the exponentially modulated sine wave fitted to the p-mode range and from the sinusoidal fit to the pseudomode range.

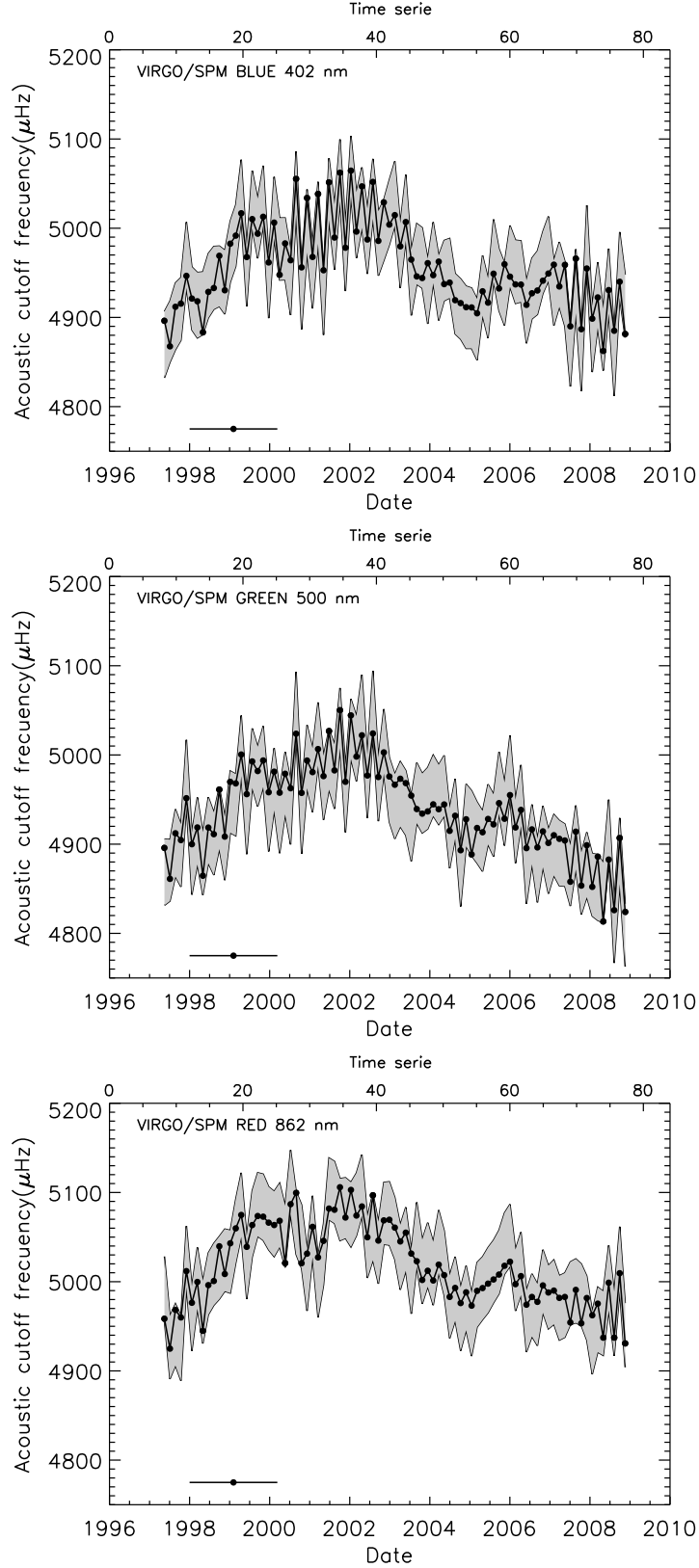


Fig. 5.— The variation of the acoustic cut-off frequency for the blue, green, and red channels of VIRGO/SPM for the 85 times series used in this research (the horizontal line centered at 1999 is the time span of the time series). Black points are the values of ν_{sc} as obtained as

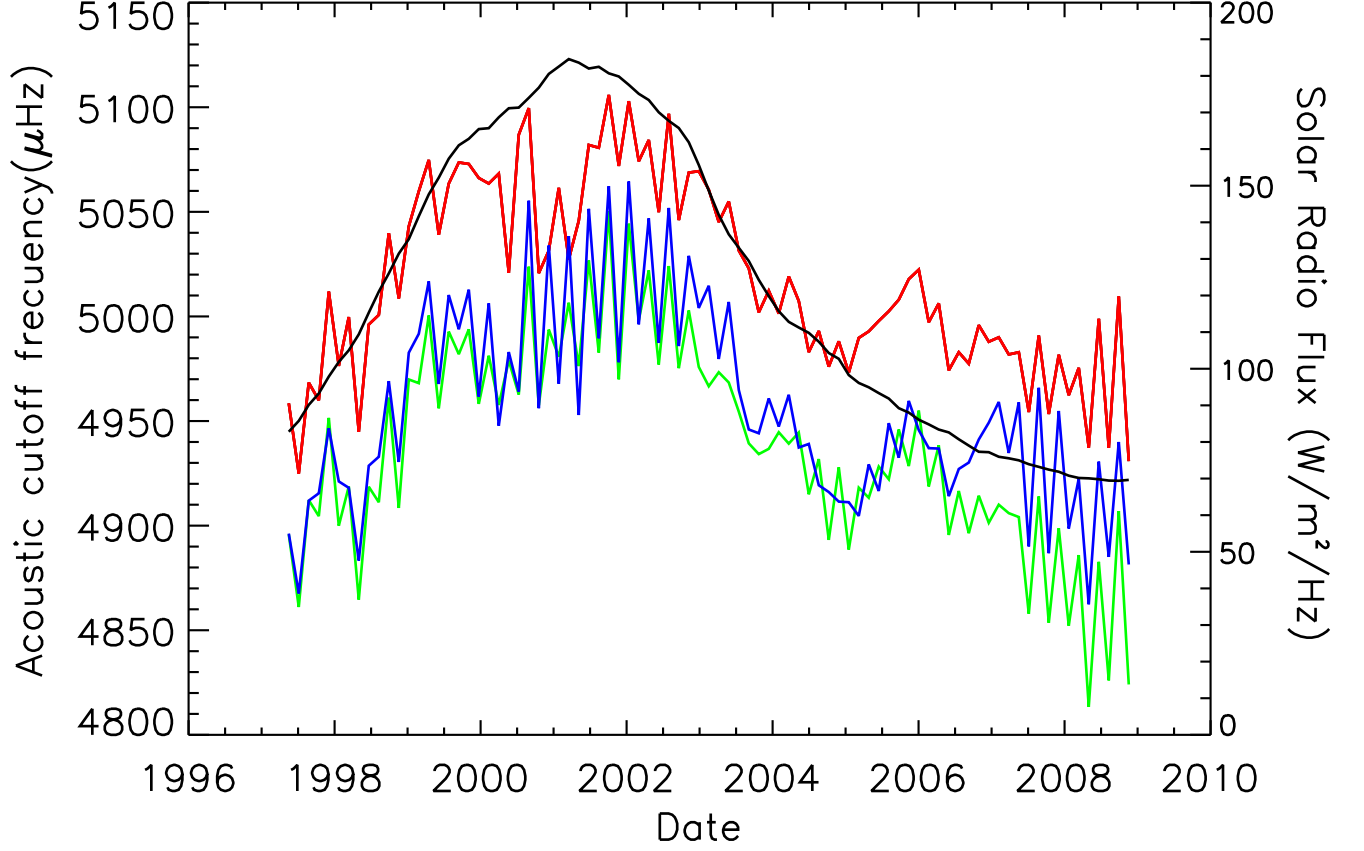


Fig. 6.— The acoustic cut-off for the red, green, and blue channels of VIRGO/SPM together with the radio flux integrated as the time series used for the ν_{ac} , average of 800 days shifting 50 days. ν_{ac} is highly correlated with the solar activity cycle (see Table 2).

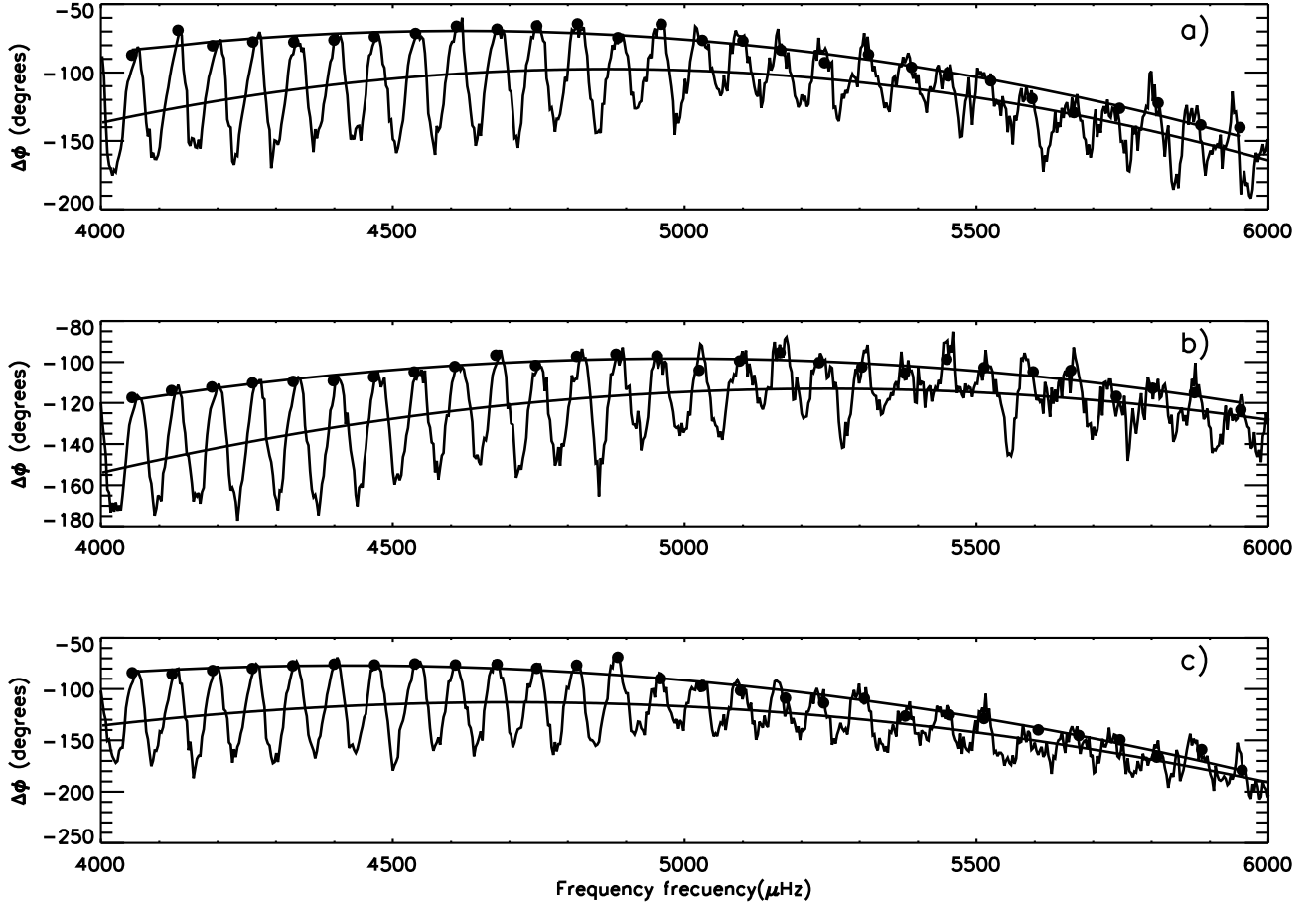


Fig. 7.— I-V phase differences in the region 4000 to 6000 μHz for three time series taken at different epochs: a) and c) in 1996 and 2009 respectively (around the minimum of the solar cycle) and b) in 2002 (around the maximum of the solar cycle). Black points are the values of phase differences just at the frequencies where the coherence function has its maxima. In each plot there are two fitted parabolas, one to the black points and the other to the whole phase difference function (see text for more details).

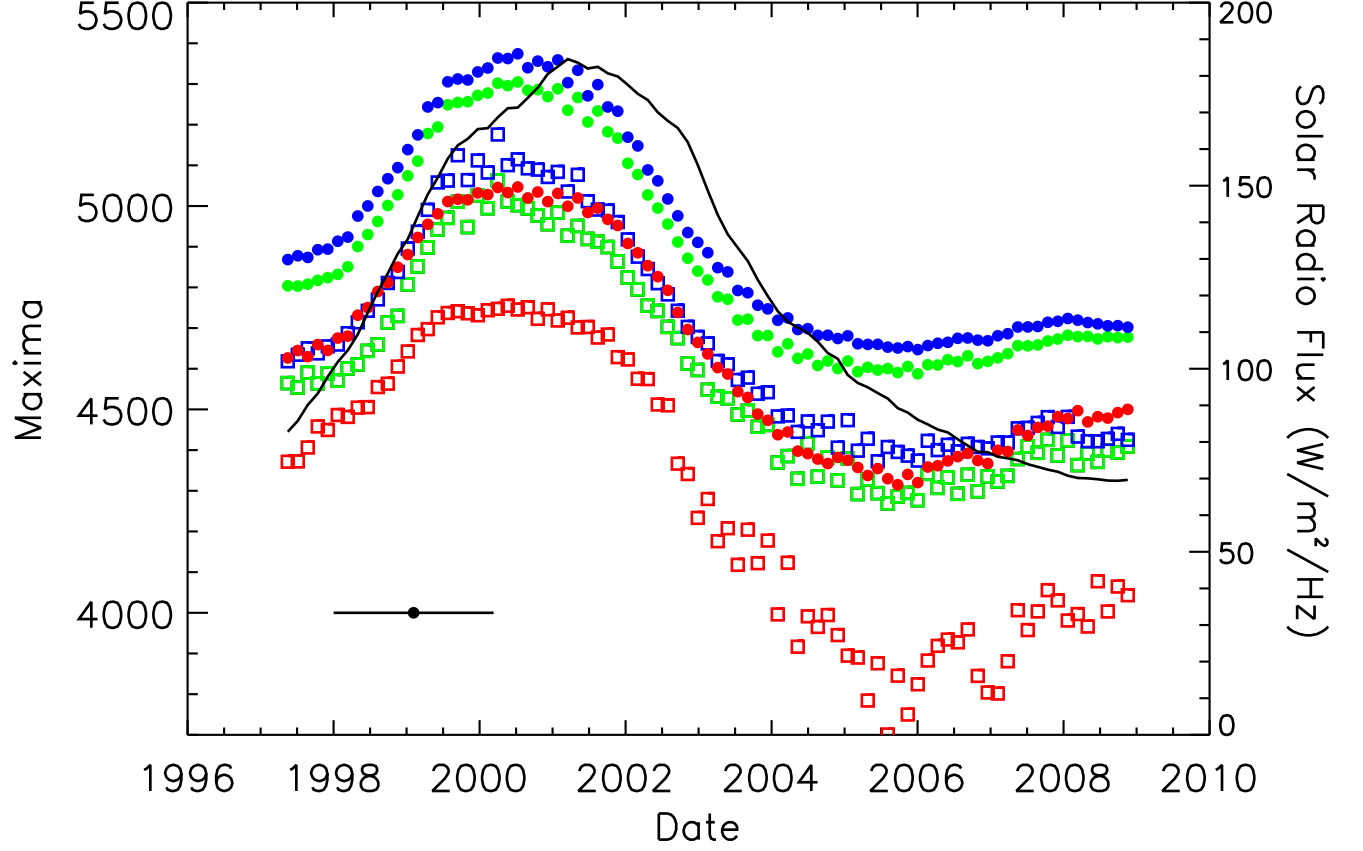


Fig. 8.— Maxima of the two parabolic fits to the phase difference functions. The different colors correspond to the three channels of VIRGO/SPM, red, green, and blue. Solid points correspond to the maxima of the fitted parabola at the whole phase difference function and open squares to the exact values of the phase differences (the black points in Figure 7). The phase differences also verify that the ν_{ac} is correlated with the solar activity cycle.

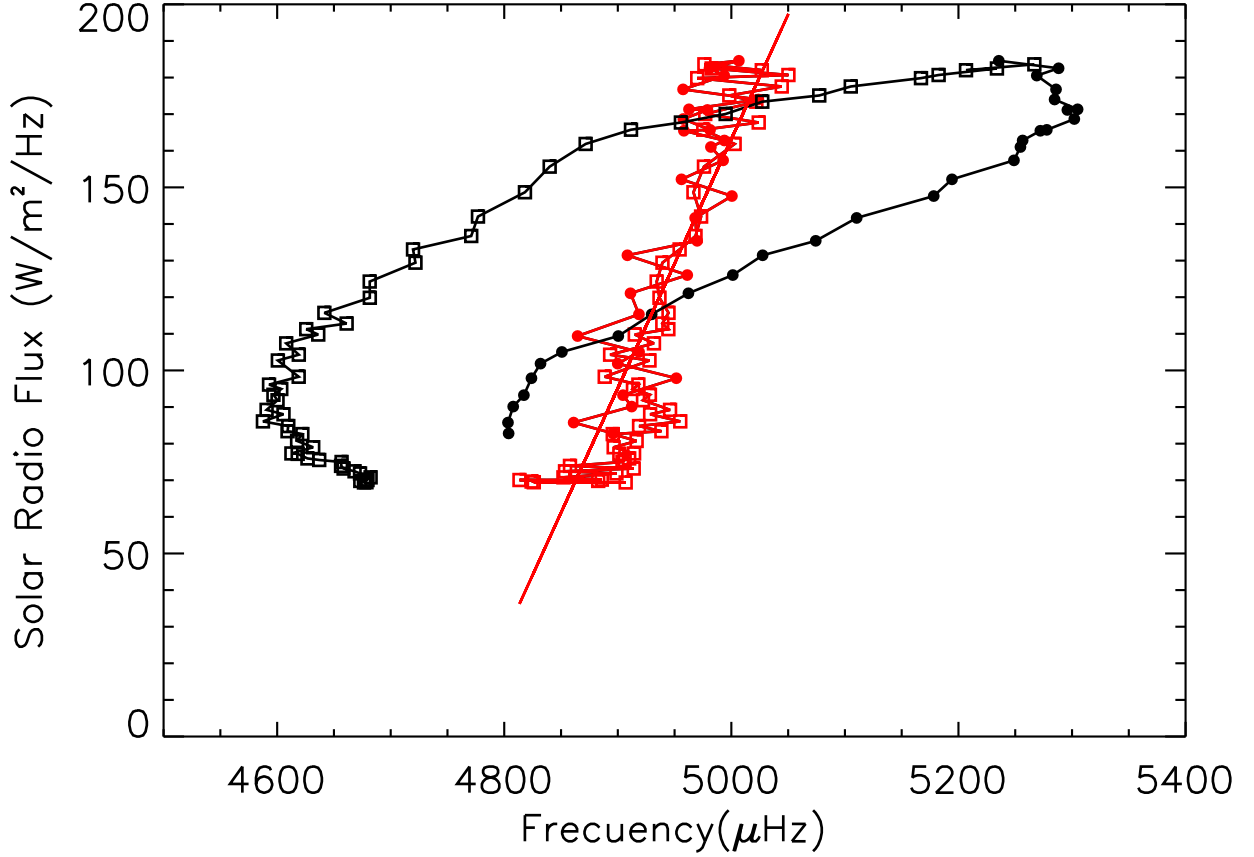


Fig. 9.— Maxima of I-V phase differences and ν_{ac} as a function of solar radio flux. Black symbols correspond to the maxima of Figure 8 for the fit to the whole phase difference function, filled circles for the ascending part of the cycle and open squares for the descending one. The maxima of the phase difference do not have a linear dependence on the solar cycle and the path in the ascending and descending parts of the cycle are different, that is, a “hysteresis” cycle. The acoustic cut-off as function of solar radio flux is plotted in red (filled circles correspond to the ascending part of the cycle and open squares to the descending one), ν_{ac} varies linearly with solar magnetic activity.